

Size-dependent asymmetric buckling of initially curved shallow nano-beam using strain gradient elasticity

Kaamran Raahemifar¹

Received: 10 September 2016 / Accepted: 19 December 2016 / Published online: 11 January 2017
© Springer-Verlag Berlin Heidelberg 2017

Abstract We have investigated the size-dependency of symmetric and asymmetric buckling in an electrostatically actuated initially curved (arch) stress-free shallow nano-beam. Using the double-mode Galerkin projection method, we have converted the partial differential equation of motion of the arch, given in the framework of Euler–Bernoulli beam and the strain gradient elasticity, to a two-degree-of-freedom model which is capable of accounting for the symmetric and asymmetric instabilities as well as the size-dependencies. Analyzing the bifurcation diagrams of the obtained reduced-order model, we have shown that the symmetric snap-through, release and pull-in instabilities, as well as the asymmetric buckling of the arch are all size-dependent. Our studies show that, as the structure scales down, possibility of the snap-through and the symmetry breaking reduces. We have derived analytical necessary conditions for prediction of the size-dependent snap-through and symmetry breaking. We further have shown that the sufficient condition for the threshold snap-through, during which the asymmetric buckling occurs prior to the symmetric snap-through, is also size-dependent.

1 Introduction

Implementation of initially curved (arch) shallow beam elements in construction of micro/nano-electro-mechanical-systems (M/NEMS) has been reported by various research

groups in recent years. Specific applications including memories (Charlot et al. 2008), sensors (Southworth et al. 2010), switches (Intaraprasong and Fan 2011), and band-pass filters (Maani Miandoab et al. 2015b; Tajaddodianfar et al. 2015b) have motivated the growing research in the field of M/NEMS with arch beam elements. Functional advantages of these systems originate from their bistability which refers to their capability to operate in two symmetric concave and convex buckled configurations at the same values of actuation parameters. Transition between these separate configurations is triggered by a precipitate motion known as the snap-through. In fact, for sufficiently curved beams, bistability occurs under the transverse load between two critical points: snap-through and release (snap-back) values (Krylov et al. 2008).

Electrostatic force, which is a popular actuation mechanism in the field of M/NEMS, enriches dynamics of the system by adding deflection-dependent nonlinearity. The beam element becomes softer as its deflection increases under the electrostatic load; while the load itself increases as a function of beam deflection. However, in a critical loading value, the structure collapses suddenly and the electrodes may stick together. This type of instability, known as the pull-in, is a characteristic of most of the electrostatically actuated M/NEMS, and is widely discussed in the literature. Zhang et al. (2014) have reviewed the extensive research performed for the study of pull-in instability in M/NEMS.

Krylov et al. (2008) and Krylov and Dick (2010) have investigated symmetric snap-through and release of the arch MEMS triggered by quasi-static or suddenly applied DC electrostatic voltages. Zhang et al. (2007) experimentally and theoretically investigated snap-through and pull-in instabilities of a bell-shaped electrostatically actuated arch. Das and Batra (2009a) continued the research on the same

✉ Kaamran Raahemifar
kraahemi@ee.ryerson.ca

¹ Department of Electrical and Computer Engineering,
Ryerson University, 350 Victoria St, Toronto, ON M5B 2K3,
Canada

system by implementation of finite element numerical methods. Other research groups have investigated the snap-through motion of the arch MEMS resonators. Younis et al. (2010) and Tajaddodianfar et al. (2015b) proposed discussions on the study of the nonlinear dynamics in an arch MEMS actuated by combined static and harmonic electrostatic actuation. Later, Tajaddodianfar et al. (2014b, 2015c, 2016a) and Maani Miandoab et al. (2015b) suggested an analytical procedure for the study of nonlinear frequency response of the MEMS resonators. Recently, they (Tajaddodianfar et al. 2015a, 2016b; Maani Miandoab et al. 2014, 2015c; Alemansour et al. 2017) have studied in detail the possibility of chaotic vibrations in this type of resonators imposed by the snap-through instabilities.

Sufficiently curved beams are also possible to present symmetry breaking which refers to appearing of non-symmetric buckling modes in their transient motion between the stable configurations. Symmetric snap-through and the possibility of accompanying asymmetric configurations are well-discussed and well-established topics in structural mechanics of macro-scaled arches (Seyranian and Elishakoff 1989; Simites 1990; Chen and Chang 2007; Plaut 2009; Camescasse et al. 2014; Plaut 2015; Amini Khoiy et al. 2016). In macro scales, these instabilities are fully parameterized by the geometry of the arch (Simites 1990; Amini Khoiy and Amini 2016). However, in contrast to the macro-scaled arches, it has been shown that the electrostatic force affects both symmetric and asymmetric buckling behaviors of the initially curved micro-beams. Krylov et al. (2008) proposed an analytical criterion for the study of snap-through instability of the MEMS stress-free bell-shaped arches which clearly reflected the nonlinearity imposed by the deflection-dependent electrostatic load. Das and Batra (2009b) numerically investigated the snap-through and pull-in instabilities, as well as the symmetry breaking, in an electrostatically loaded shallow micro arch. Later, Krylov et al. (2011) and Tajaddodianfar et al. (2014a) studied the structural stability of a free-of-pull-in initially curved micro-beam actuated by fringing electrostatic fields. They proposed the possibility of appearing non-symmetric buckling modes based on their computational methods. Using reduced order mathematical models consisting of the first symmetric and asymmetric mode shapes, Medina et al. (2012) explored in detail the structural stability of stress-free micro-arches actuated by either deflection-independent mechanical or deflection-dependent electrostatic loads. Based on the bifurcation study of their models, they derived analytical expressions for prediction of the symmetric snap-through and asymmetric buckling of the arch, arguing that for sufficiently curved beams asymmetric instabilities are possible to occur prior to symmetric snap-through. Thus, validity of the reduced order models consisting only the first symmetric mode will

be undermined for the sufficiently curved arches (Medina et al. 2012). Later, they (Medina et al. 2014b) extended their studies of symmetry breaking and snap-through to pre-stressed initially curved micro-beams. They (Medina et al. 2014a) also have recently reported experimental investigations for symmetric and asymmetric buckling of the arch micro-beams.

Various advantages, including higher natural frequencies and faster responses, motivate extensive research for scaling down the micro structures and constructing nano-scaled systems. However, many experimental observations have shown that, as the smallest dimension of the system decreases below a few microns, the conventional continuum theories fail to accurately address the nonlinear behavior of NEMS (Wang et al. 2008). For example, Namazu et al. (2000) have experimentally observed that as the thickness of silicon beams decrease below 255 nm their bending stiffness increases by a factor of four. Also, due to Fleck et al. (1994), torsion stiffness of copper wires increase by a factor of three as their diameter decrease from 170 to 12 μm . Based on such observations, in contrast to classic continuum theories, elastic properties of material vary as a function of its size. To account for these size-dependencies, non-classic continuum theories including the strain gradient (Kong et al. 2009; Mustapha and Ruan 2015), modified couple stress (Ghayesh et al. 2013; Akgöz and Civalek 2013; Farokhi et al. 2013), surface energy (Fu et al. 2010; Nejat Pishkenari et al. 2015), and nonlocal stress (Reddy 2010) theories have been developed in recent years. In the past few years, several investigations have been conducted to understand the size-dependent nature of the nano-beams statics and dynamics (Wang et al. 2011; Akgöz and Civalek 2013). It is worth noting that various strain gradient theories are reported in the literature; however, throughout this paper, when using the term “strain gradient theory”, we refer to the theory developed by Lam et al. (2003). Recently, Tajaddodianfar et al. (2015d) have proposed a strain gradient continuum model based on the Euler–Bernoulli and shallow arch assumptions for the study of size-dependent nonlinear phenomena in the initially curved nano-beams. They have shown that the snap-through and pull-in instabilities in the shallow nano-arches are size-dependent, as predicted by the strain gradient theory (Tajaddodianfar et al. 2015d). Moreover, as the nano-arch scales down the minimum initial rise parameter required for the possibility of symmetric snap-through increases (Tajaddodianfar et al. 2015d).

Benefiting from the combined functional advantages of initially curved beams and nano-scale systems motivates us to investigate, in this paper, the influence of size on the structural dynamics of initially curved shallow nano-beams. To the authors’ best knowledge, size-dependent asymmetric

buckling of shallow nano-arches has not been thoroughly investigated in the literature. We aim in this paper to scrutinize the size-dependent snap-through and pull-in instabilities as well as the size-dependent symmetry breaking in the stress-free shallow nano-arches. In this regard, this paper extends the previous knowledge of the structural stability of initially curved beams to the nano-scale where the conventional continuum theories, which have been used so far e.g. by Medina et al. (2012), fail to account for size-dependencies. Additionally, this work is an extension to a previous work by Tajaddodianfar et al. (2015d) where they have limited their discussions to the presentation of the strain gradient model and the corresponding single-degree-of-freedom reduced-order model which is capable of accounting only for the symmetric instabilities. In summary, in this paper we focus on the size-dependent asymmetric structural instabilities of the shallow nano-arches.

Toward our aim, we first use the double-mode Galerkin projection method to derive the two-degree-of-freedom reduced-order strain gradient model which governs the transverse motion of the nano-arch. Using three-dimensional bifurcation diagrams, we investigate the symmetric and asymmetric buckling of the nano-arch, showing that the critical values describing the limit point snap-through, release and pull-in, as well as the symmetry breaking, are all size dependent. Later, we derive analytical expressions for description of the minimum required value for the

initial curvature to facilitate the size-dependent symmetric and asymmetric buckling.

In the rest of this paper, we propose the mathematical reduced order models in Sect. 2. Then in Sect. 3 we propose our bifurcation studies on the obtained models. In Sect. 4 we propose our study of the arch’s nonlinear behaviors in its parameter space. Derivation of analytical expressions and conclusions are given in Sects. 5 and 6, respectively.

2 Mathematical modeling

An initially curved beam of length L , width w and thickness d , clamped at the two ends, is considered under the static DC electrostatic load distributed over the beam length, as shown in Fig. 1. We suppose that the initial deflection of the beam is described by a function $w_0(x)$, while the load-dependent deflection of it is given by a function $w(x)$, measured from the x axis as shown in Fig. 1. Using the parameters given in Table 1, and based on the shallow arch and Euler–Bernoulli beam assumptions ($h_0 \ll L, d \ll L$), the equilibrium equations of the stress-free arch using the strain gradient elasticity theory are given as (Tajaddodianfar et al. 2015d):

$$\frac{\partial}{\partial x} \left[\tilde{E}A \left(\frac{1}{2} \left(\frac{\partial w}{\partial x} \right)^2 - \frac{1}{2} \left(\frac{dw_0}{dx} \right)^2 \right) \right] = 0, \tag{1}$$

Fig. 1 Schematics of electrostatically actuated initially curved shallow nano-beam clamped at both ends

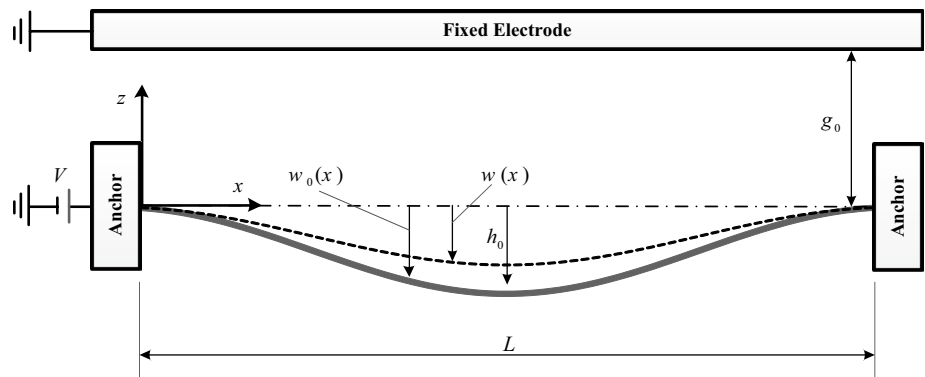


Table 1 Nomenclature

Symbol	Description	Unit	Symbol	Description	Unit
b	Width	m	G	Shear modulus	Pa
g_0	Fixed gap between electrodes	m	l_0	Material parameter for dilatation gradients	m
h_0	Initial elevation	m	l_1	Material parameter for deviatoric stretch gradients	m
d	Thickness	m	l_2	Material parameter for rotation gradient	m
A	Cross sectional area	m ²	ν	Poisson’s ratio	–
E	Young’s modulus	Pa	V	Electrostatic voltage	V
\tilde{E}	Effective Young’s modulus	Pa			

$$-K \left(\frac{\partial^6 w}{\partial x^6} - \frac{\partial^6 w_0}{\partial x^6} \right) + S \left(\frac{\partial^4 w}{\partial x^4} - \frac{d^4 w_0}{dx^4} \right) - \frac{\partial}{\partial x} \left\{ \frac{\partial w}{\partial x} \left[\tilde{E}A \left(\frac{1}{2} \left(\frac{\partial w}{\partial x} \right)^2 - \frac{1}{2} \left(\frac{dw_0}{dx} \right)^2 \right) \right] \right\} = \frac{-\varepsilon_0 b V^2}{2(g_0 + w)} \quad (2)$$

where:

$$K = GI \left(2l_0^2 + \frac{4}{5} l_1^2 \right) \quad (3)$$

$$S = \tilde{E}I + GA \left(2l_0^2 + \frac{8}{15} l_1^2 + l_2^2 \right) \quad (4)$$

with $\tilde{E} = E/(1 - \nu^2)$ and other parameters are given in Table 1. Boundary conditions are also given as:

$$\begin{aligned} w(0) = w(L) = 0, \\ \left. \frac{\partial w}{\partial x} \right|_{x=0} = \left. \frac{\partial w}{\partial x} \right|_{x=L} = 0, \\ \left. \frac{\partial^3 w}{\partial x^3} \right|_{x=0} = \left. \frac{\partial^3 w}{\partial x^3} \right|_{x=L} = 0 \end{aligned} \quad (5)$$

Regarding that the Eq. (1) implies constant deflection-dependent axial force along the beam, Eqs. (1) and (2) are converted to the following single equation (Tajaddodianfar et al. 2015d):

$$-K \left(\frac{\partial^6 w}{\partial x^6} - \frac{d^6 w_0}{dx^6} \right) + S \left(\frac{\partial^4 w}{\partial x^4} - \frac{d^4 w_0}{dx^4} \right) - \frac{\partial^2 w}{\partial x^2} \left[\frac{\tilde{E}A}{2L} \int_0^L \left[\left(\frac{\partial w}{\partial x} \right)^2 - \left(\frac{dw_0}{dx} \right)^2 \right] dx \right] = \frac{-\varepsilon_0 b V^2}{2(g_0 + w)} \quad (6)$$

with the boundary conditions (5).

Using the non-dimensional quantities given in Table 2, one can convert Eq. (6) to the following dimensionless counterparts:

$$\begin{aligned} \theta_0 \left(\frac{\partial^6 \hat{w}}{\partial \hat{x}^6} - \frac{d^6 \hat{w}_0}{d\hat{x}^6} \right) + \left(\frac{\partial^4 \hat{w}}{\partial \hat{x}^4} - \frac{d^4 \hat{w}_0}{d\hat{x}^4} \right) \\ - \theta_1 \frac{\partial^2 \hat{w}}{\partial \hat{x}^2} \left[\int_0^1 \left[\left(\frac{\partial \hat{w}}{\partial \hat{x}} \right)^2 - \left(\frac{d\hat{w}_0}{d\hat{x}} \right)^2 \right] d\hat{x} \right] = \frac{-\beta}{(1 + \hat{w})^2} \end{aligned} \quad (7)$$

with the nondimensionalized boundary conditions:

$$\begin{aligned} \hat{w}(0) = \hat{w}(1) = 0, \\ \left. \frac{d\hat{w}}{d\hat{x}} \right|_{\hat{x}=0} = \left. \frac{d\hat{w}}{d\hat{x}} \right|_{\hat{x}=1} = 0, \\ \left. \frac{d^3 \hat{w}}{d\hat{x}^3} \right|_{\hat{x}=0} = \left. \frac{d^3 \hat{w}}{d\hat{x}^3} \right|_{\hat{x}=1} = 0 \end{aligned} \quad (8)$$

Table 2 Dimensionless parameters

$\hat{x} = \frac{x}{L}$	$h = \frac{h_0}{g_0}$	$\hat{d} = \frac{d}{g_0}$
$\hat{w} = \frac{w}{g_0}$	$\hat{w}_0 = \frac{w_0}{g_0}$	$\theta_1 = \frac{\tilde{E}bdg^2}{2S}$
$\hat{b} = \frac{b}{g_0}$	$\theta_0 = \frac{-K}{SL^2}$	$\beta = \frac{\varepsilon_0 b L^4 V^2}{2g^3 S}$

2.1 Reduced order model

The Galerkin decomposition is employed to convert the governing Eq. (7) to the reduced-order (RO) model which will be more convenient for the study of snap-through, pull-in and symmetry breaking in the investigated shallow nano-arch. The procedure starts with assuming the deflection of the arch to be approximated by finite-term weighted sum of base functions:

$$\hat{w}(\hat{x}) = \sum_{n=1}^N q_n \varphi_n(\hat{x}) \quad (9)$$

where N is the number of considered base functions $\varphi_n(\hat{x})$ which represent mode shapes of the shallow double clamped nano-arch satisfying the boundary conditions (8).

For a straight double clamped strain gradient beam ($w_0 = 0$), the mode shapes are obtained as solutions for the following Eigen-value problem:

$$\theta_0 \frac{d^6 \varphi_n}{d\hat{x}^6} + \frac{d^4 \varphi_n}{d\hat{x}^4} - k_n \varphi_n(\hat{x}) = 0, \quad (10)$$

with the boundary conditions (8) and with k_n as the n -th eigen-value. Maani Miandoab et al. (2015a) have proposed discussions on the solution of Eq. (10) for $\varphi_n(\hat{x})$ and k_n . They have shown that for very small values of θ_0 , the solution of Eq. (10) meets those of the following Eigen-value problem which governs the mode shapes of the classical double clamped straight beam:

$$\frac{d^4 \varphi_n}{d\hat{x}^4} - k_n \varphi_n(\hat{x}) = 0, \quad (11)$$

with the first two of boundary conditions (8). However, although the solution for (11) does not satisfy the 3rd of boundary conditions (8), but the difference between the solutions of (10) and (11) is negligible, provided that $\theta_0 \ll 1$. For instance, for a typical silicon arch with the parameters given in Table 3, $\theta_0 = -4.4 \times 10^{-8}$ is calculated. Thus, implementation of the mode shapes of the classical straight beam instead of that of the strain gradient straight beam is justified for very small θ_0 . Additionally, due to negligible encountered error, most researchers employ the mode shapes of straight beam for the analysis of shallow arches (Krylov et al. 2008; Krylov and Dick 2010; Younis et al. 2010). With all these discussions, we

Table 3 Typical values for the material and geometrical parameters of the nano-arch

Parameter	Value
Young modulus	$E = 165$ Gpa
Poison ratio	$\nu = 0.06$
Nano-arch length	$L_0 = 500$ μm
Nano-arch width	$b_0 = 30$ μm
Nano-arch thickness	$d_0 = 1$ μm
Gap between the electrodes	$g_0 = 5$ μm

make use of the mode shapes of the classical straight double clamped beam, governed by (11), as the base functions in Eq. (9):

$$\varphi_n(\hat{x}) = C_n \left[\cosh(k_n \hat{x}) - \cos(k_n \hat{x}) - \left(\frac{\cosh(k_n) - \cos(k_n)}{\sinh(k_n) - \sin(k_n)} \right) (\sinh(k_n \hat{x}) - \sin(k_n \hat{x})) \right],$$

$$k_1 = 4.7300, k_2 = 7.8532, \dots \tag{12}$$

with C_n as a normalizing coefficient which guarantees $\max\{\varphi_n(\hat{x})\}_{\hat{x} \in [0,1]} = 1$.

Supposing the initial curvature of the arch to be given by the first mode shape, $w_0(\hat{x}) = h\varphi_1(\hat{x})$, we substitute (9) in (7), multiply both sides by $\varphi_n(\hat{x})$ and integrate over the arch length. Regarding the orthogonality of mode shapes, and setting $N = 2$, we can obtain the following two degrees-of-freedom model governing the equilibrium of the strain gradient shallow arch under electrostatic actuation:

$$(b_{11} + \theta_0 n_{11})(q_1 - h) + \theta_1 s_{11}^2 q_1 (q_1^2 - h^2) + \theta_1 s_{11} s_{22} q_1 q_2^2 + \beta \int_0^1 \frac{\varphi_1}{(1 + q_1 \varphi_1 + q_2 \varphi_2)^2} dx = 0, \tag{13}$$

$$(b_{22} + \theta_0 n_{22})q_2 + \theta_1 s_{11} s_{22} q_2 (q_1^2 - h^2) + \theta_1 q_2^3 s_{22}^2 + \beta \int_0^1 \frac{\varphi_2}{(1 + q_1 \varphi_1 + q_2 \varphi_2)^2} dx = 0 \tag{14}$$

where we have:

$$b_{ij} = \int_0^1 \varphi_i'' \varphi_j'' d\hat{x},$$

$$s_{ij} = \int_0^1 \varphi_i' \varphi_j' d\hat{x}, \tag{15}$$

$$n_{ij} = \int_0^1 \varphi_i \frac{d^6 \varphi_j}{d\hat{x}^6} d\hat{x}$$

Using the mode shapes given by (12), the above constants are found as: $b_{11} = 198.463$, $b_{22} = 1669.859$, $n_{11} = -2441.6$, $n_{22} = -7692.0$, $s_{11} = 4.878$, and

$s_{22} = 20.218$. Note that with the assumption $\theta_0 \ll 1$ we can replace $b_{11} + \theta_0 n_{11}$ and $b_{22} + \theta_0 n_{22}$ by b_{11} and b_{22} , respectively. Moreover, since the nonlinear integrals arising in Eqs. (13) and (14) cannot be treated analytically, we Taylor expand them about $q_2 = 0$ up to the first order. This yields a simpler form of the reduced order model which seems similar to what is already reported by Medina et al. (Medina et al. 2012) for the classical arch:

$$b_{11}(q_1 - h) + \theta_1 s_{11}^2 q_1 (q_1^2 - h^2) + \theta_1 s_{11} s_{22} q_1 q_2^2 + \beta I_1(q_1) = 0, \tag{16}$$

$$[b_{22} + \theta_1 s_{11} s_{22} (q_1^2 - h^2) + \theta_1 q_2^2 s_{22}^2 - \beta I_2(q_1)] q_2 = 0 \tag{17}$$

where we have:

$$I_1(q_1) = \int_0^1 \frac{\varphi_1}{(1 + q_1 \varphi_1)^2} d\hat{x},$$

$$I_2(q_1) = \int_0^1 \frac{2\varphi_2^2}{(1 + q_1 \varphi_1)^3} d\hat{x}, \tag{18}$$

$$\int_0^1 \frac{\varphi_1 \varphi_2}{(1 + q_1 \varphi_1)^3} d\hat{x} = 0,$$

$$\int_0^1 \frac{\varphi_2}{(1 + q_1 \varphi_1)^2} d\hat{x} = 0,$$

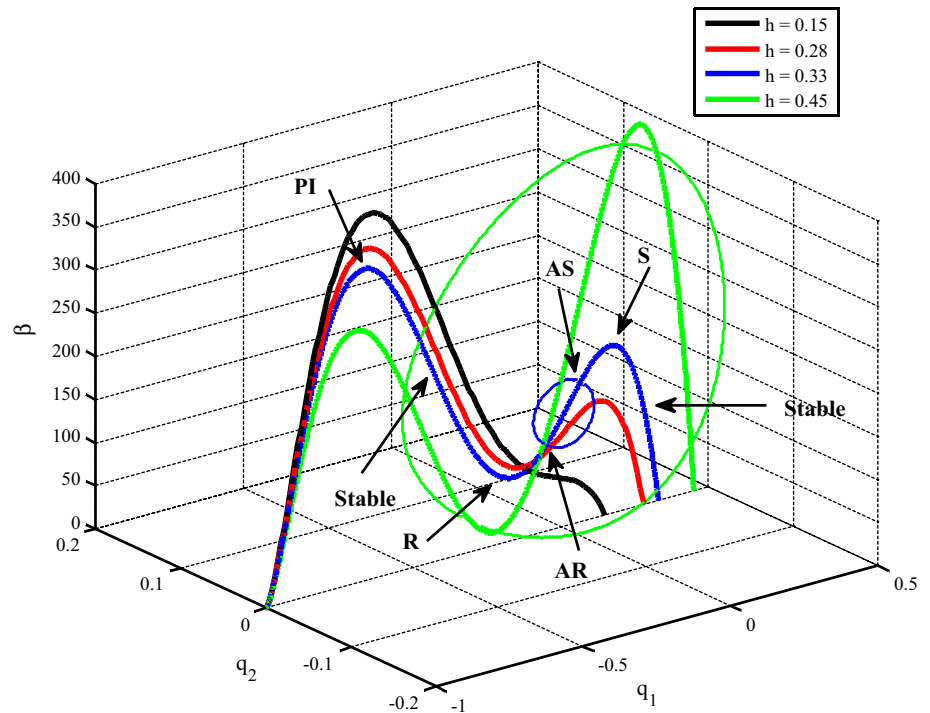
Note that Eq. (16) governs the first symmetric mode shape of the arch, while Eq. (17) is associated with the second mode shape; therefore, nonzero value for q_2 implies asymmetric behaviors of the arch. Also, knowing that the stretching parameter θ_1 and the voltage parameter β are both size-dependent, we aim to investigate the size-dependent pull-in, snap-through and symmetry breaking of the shallow nano-arch, using Eqs. (16) and (17).

3 Bifurcation analysis

3.1 Bifurcation diagrams with the classical theory

As the first step toward the analysis of size-dependent nonlinear behaviors of the investigated nano-arch, we need to analyze the bifurcation diagram of the fixed points associated with the 2-DOF model given by Eqs. (16) and (17). Since the nonlinear integrals do not have closed form solutions, the bifurcation diagrams are plotted numerically. To this aim, we first mention that $q_2 = 0$ is a trivial solution for Eq. (17); thus, setting $q_2 = 0$ in Eq. (16), prescribing values for q_1 and solving (16) for β , one can derive the bifurcation diagram associated with the first symmetric mode shape of the arch (see Fig. 2). Such a bifurcation diagram, which is plotted in $q_2 = 0$ plane, is always a solution for the 2-DOF model, and governs the symmetric nonlinear behaviors including pull-in, symmetric snap-through and symmetric release, and has been a subject of various previous studies

Fig. 2 Bifurcation diagram of fixed points, with the classical theory, for the typical parameters given in Table 3 and associated with four values of the initial rise parameter. Pull-in (PI), symmetric snap-through (S) and release (R), asymmetric snap-through (AS) and release (AR), as well as the stable branches of the diagram are pointed in the *blue-colored diagram*. These critical points have similar counterparts in other diagrams. See the text for further discussion (color figure online)



(Krylov et al. 2008; Krylov and Dick 2010; Tajaddodianfar et al. 2015a). As the main results of these previous works, we can enumerate some of the bold points which will be used later in this paper:

- The electrostatically actuated arch always experience the pull-in instability which is represented by a pull-in bifurcation point (PI) with the property $d\beta/dq_1 = 0$ (all curves in Fig. 2).
- Provided that the initial elevation of the arch is larger than a critical value, $h_S < h$, the arch undergoes symmetric snap-through at a bifurcation point (S) with the property $d\beta/dq_1 = 0$. The symmetric release, or snap-back, is also represented by a bifurcation point (R) (all curves except $h = 0.15$ in Fig. 2).

For the study of asymmetric behaviors with $q_2 \neq 0$ values, we first solve Eq. (17) for the nontrivial value of $q_2^2(q_1, \beta)$ and substitute it in Eq. (16); then, with a prescribed value of q_1 , we solve the obtained equation for β . The prescribed value for q_1 and the obtained value for β is put back into Eq. (17), solving it for q_2 ; a real value of which stands for the asymmetric snap-through and release. Medina et al. (2012) have already studied the symmetric and asymmetric instabilities of the shallow arch, adding to the above points that:

- Provided that the initial elevation of the arch is larger than another critical value, $h_S < h_{AS} < h$, the asymmetric equilibrium points with the property $q_2 \neq 0$ bifurcate

from the unstable branch of the symmetric bifurcation diagram via the bifurcation points AS and AR, associated with asymmetric snap-through and asymmetric release, respectively (curves associated with $h = 0.33$ and $h = 0.45$ in Fig. 2).

- For values of the initial elevation parameter larger than a third threshold value $h_S < h_{AS} < h_{TS} < h$ the asymmetric bifurcation points, AS and AR, move from the unstable branch to the stable branch of the symmetric bifurcation diagram; imposing the asymmetric snap-through to take place at the loading values smaller than the corresponding loading value associated with symmetric buckling. Thus, in this case, the asymmetric points AS and AR are the critical instability points ($h = 0.45$ curve in Fig. 2).

Figure 2, displays the equilibrium values of the voltage parameter β versus q_1 and q_2 for several values of the initial rise parameter h , and for the parameter values associated with a typical shallow arch given in Table 3. Note that Fig. 2 is obtained with the classical theory which implies the material length scale parameters equal to zero.

3.2 Bifurcation diagrams with the strain gradient theory

In order to study the size-dependent nature of the described bifurcation diagrams based on the strain gradient theory, we scale the nano-arch given in Table 3 by several scaling factors. Then, for each scaled nano-arch we compute

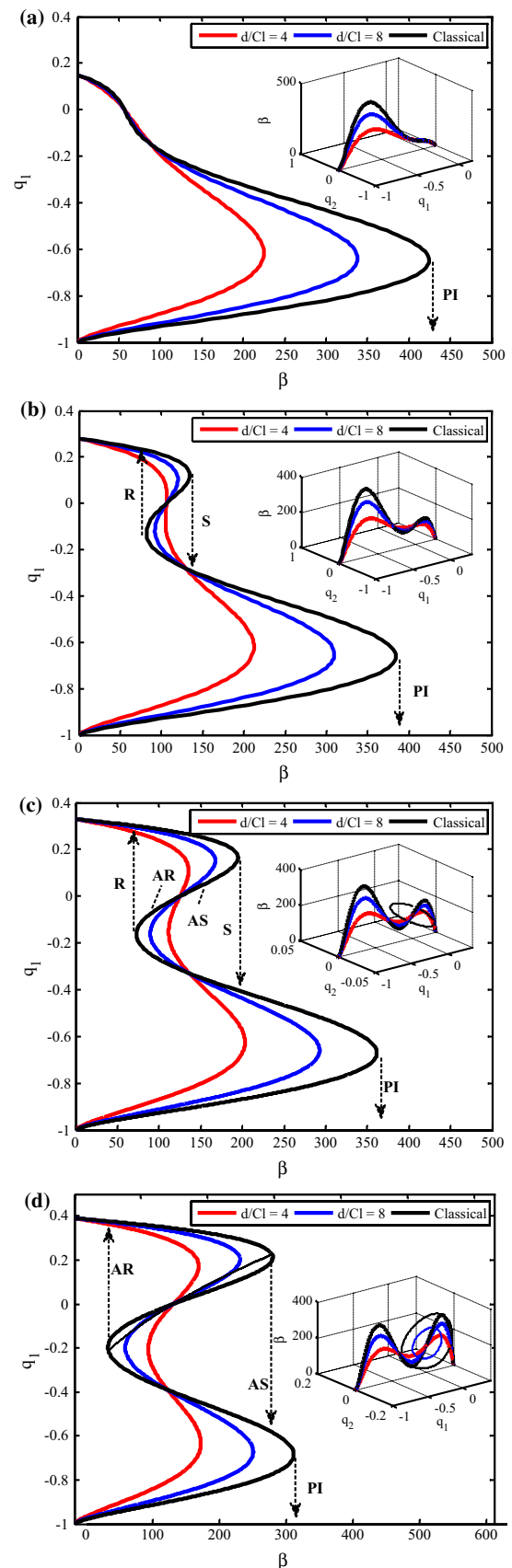
Fig. 3 Two-dimensional bifurcation diagrams obtained by the classical and strain gradient theories for two separate values of d/Cl ratio. The three-dimensional counterparts are shown as the insets. The critical pull-in (PI), symmetric snap-through (S) and release (R), asymmetric snap-through (AS) and release (AR) are all shown on the classical diagram. These points have non-classical analogues. All parts are obtained for the scaled values of the parameters given in Table 3 and with **a** $h = 0.15$, **b** $h = 0.28$, **c** $h = 0.33$ and **d** $h = 0.39$

the corresponding size-dependent parameter θ_1 and employ it for derivation of the corresponding bifurcation diagram. We suppose three equal material length scale parameters, $l_0 = l_1 = l_2 = Cl$, taking $Cl = 100$ nm. Note that as the thickness of the nano-arch is varied by scaling, geometrical ratios $L/d, b/d$ and g/d are all preserved; thus, the classical theory, with zero length scale parameter, yields equal non-dimensional parameters for all of the scaled nano-arches, and results in the same bifurcation diagram regardless of the size. However, regarding the nonzero length scale parameters, the bifurcation diagrams vary depending on the scale and size of the nano-arch. Thus, for each of the bifurcation diagrams predicted by the classical theory for the given value of the initial rise parameter h , as in Fig. 2, the strain gradient theory predicts size-dependent bifurcation diagrams.

Figure 3 describes the size-dependent bifurcation diagrams associated with the classical ones shown in Fig. 2. The two-dimensional plots in Fig. 3 display the $q_2 = 0$ section of the three-dimensional diagram which is also shown as the inset in each figure. Figure 3a, with $h = 0.15$, represents the case where both the classical and non-classical theories predict the pull-in as the only instability of the nano-arch. However, as the nano-arch scales down, the non-dimensional pull-in voltage decreases. For the deeper nano-arches displaying bistability, as in Fig. 3b with $h = 0.28$, the strain gradient theory predicts reduction in symmetric pull-in and snap-through values of β , while the corresponding value for the symmetric release increases. Thus, as the nano-arch scales down, its bistable property fades. This is more transparent in Fig. 3b for $d/Cl = 4$ where the strain gradient theory predicts an almost zero-width bistable interval over the β axis; while the classical theory predicts the nano-arch to be bistable.

Figure 3c with $h = 0.33$ illustrates the case where the classical theory predicts emerging of the symmetry breaking from the bifurcation points AS and AR. However, the strain gradient theory does not predict symmetry breaking for the scaled nano-arches in this case. This shows that the symmetry breaking behavior of the nano-arch is size-dependent, as well as the symmetric instabilities of it.

As the initial elevation of the nano-arch increases, the bifurcation points AS and AR move toward the stable



branches of the bifurcation diagram, and eventually, they pass the critical points S and R, where the asymmetric instability becomes practically critical. Emerging of the bifurcation points AS and AR and their move toward the stable branches are all size-dependent. As detectable from Fig. 3d for $h = 0.39$, while the classical theory predicts the points AS and AR to be almost coincided with the points S and R, respectively, the strain gradient theory predicts that for very small scales of the nano-arch, $d/Cl = 4$, the symmetry breaking is still absent. Nevertheless, for larger sized nano-arch with $d/Cl = 8$, the strain gradient theory predicts emerging of AS and AR bifurcation points which are still located on the unstable branch of the corresponding bifurcation diagram.

Plots in Fig. 3 show that, at each case, the classical and size-dependent bifurcation diagrams share two inflection points; each of which located on one of the stable and unstable branches of the bifurcation diagram. Moreover, Fig. 3d shows that the mathematical surface constructed by the asymmetric branches of the classical bifurcation diagram and its non-classical counterpart share a gradient vector which is also perpendicular to the q_2 axis. However, our observations proposed in Fig. 3 prove that both symmetric and asymmetric behaviors of the nano-arch are size-dependent. In the next section, we analytically investigate the symmetric and asymmetric instabilities of the nano-arch, as well as the critical values h_S , h_{AS} and h_{TS} .

4 Nonlinear behaviors in parameter space

4.1 Symmetric behaviors

For the study of the symmetric and asymmetric instabilities, we refer again to the 2-DOF model given by Eqs. (16) and (17). Noticing that $q_2 = 0$ is always a solution contributing to the symmetric behaviors, the first-mode Eq. (16) is linearized about $q_2 = 0$ yielding (Medina et al. 2012):

$$b_{11}(q_1 - h) + \theta_1 s_{11}^2 q_1 (q_1^2 - h^2) + \beta I_1 (q_1) = 0, \tag{19}$$

which governs the first-mode bifurcation diagram. Solving this equation for β and setting $d\beta/dq_1 = 0$, one can derive the following equation; the roots of which contribute to the pull-in (PI) and symmetric snap-through (S) and release (R) points (Medina et al. 2012).

$$\theta_1 s_{11}^2 q_1^2 (I_1' q_1 - 3I_1) + (I_1' q_1 - I_1)(b_{11} - \theta_1 s_{11}^2 h^2) - b_{11} I_1' h = 0 \tag{20}$$

where (') denotes differentiation with respect to q_1 . One can obtain the critical pull-in and symmetric snap-through and release curves by prescribing values for q_1 and solving Eq. (20) for h . The set of (q_1, h) obtained in this way is fed to Eq. (19) for obtaining the corresponding critical value

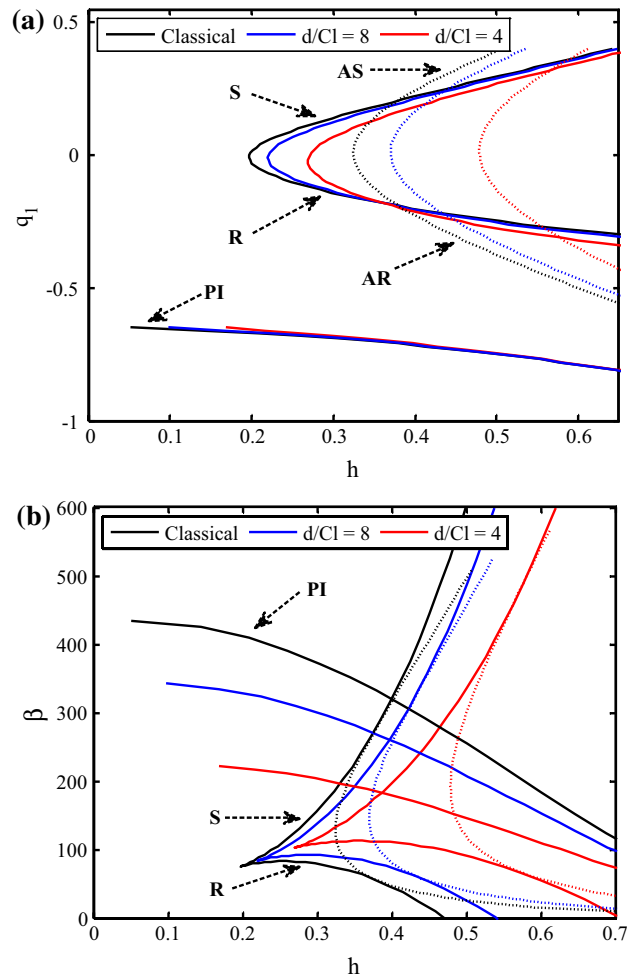


Fig. 4 a Critical values of q_1 associated with pull-in (PI), symmetric snap-through (S) and release (R) instabilities versus the initial elevation parameter h , obtained from Eq. (20) and shown by solid curves, together with the critical values of the asymmetric snap-through (AS) and release (AR) given by Eq. (21) and depicted by dotted curves. Results are obtained both with the classical theory and two scaled structures contributing to the strain gradient theory. b Corresponding values of β versus h

for β . Note that with the size-dependent nature of parameter θ_1 , this procedure results in various curves associated with pull-in, snap-through and release branches at each scale. Figure 4a displays the critical values of q_1 versus h for various scales of the typical nano-arch given in Table 3. Also, Fig. 4b depicts the corresponding critical values of β versus h .

Noting that Eq. (20) is quadratic in h , one can find the minimum value of the initial elevation parameter, required for the possibility of symmetric snap-through and release, by solving Eq. (20) for h and differentiating it with respect to q_1 ; solving $dh/dq_1 = 0$ and substituting the resulting value of q_1 back into Eq. (20), one can obtain the minimum value of h required for bistability of the nano-arch,

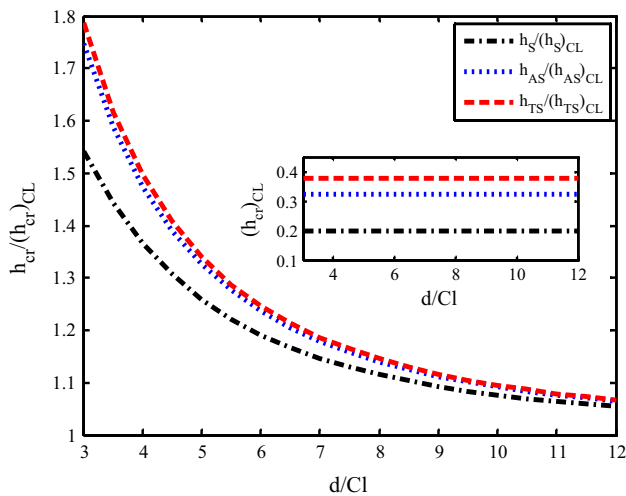


Fig. 5 Normalized values of the minimum initial rise parameter required for symmetric snap-through (h_S), asymmetric snap-through (h_{AS}) and threshold snap-through (h_{TS}) given by the strain gradient theory versus the d/Cl ratio. Corresponding constant values given by the classical theory are shown as the inset

h_S . Regarding the size-dependency of θ_1 , we can obtain h_S for each value of the ratio d/Cl , and depict it in Fig. 5. Note that, despite the classical theory which predicts a constant value of h_S , the strain gradient theory predicts that h_S increases as the nano-structure scales down.

4.2 Asymmetric behaviors

Since the asymmetric bifurcation points AS and AR arise on the symmetric bifurcation diagram governed by (19), these points are obtained by simultaneous solving of Eqs. (17) and (19). To this aim, β is found from (19) and is substituted in (17) with $q_2 \neq 0$. This yields the following equation governing the asymmetric critical points:

$$I_1(b_{22} + \theta_1 s_{11} s_{22}(q_1^2 - h^2) + 2I_2(q_1 - h)(b_{11} + \theta_1 s_{11}^2 q_1(q_1 + h))) = 0 \tag{21}$$

Prescribing values for q_1 and solving Eq. (21) for h , one can find the critical values of q_1 versus h corresponding to the asymmetric bifurcation points AS and AR. Feeding these values back into Eq. (19) one can find the corresponding values of β versus h . Additionally, depending on the scaling parameter, we expect size-dependent values for the critical points AS and AR. This is shown in Fig. 4a and 4b, too.

Regarding Fig. 4a, for finding the minimum value of h required for the possibility of symmetry breaking h_{AS} , we solve Eq. (21) for h and equate $dh/dq_1 = 0$; substituting the obtained value for q_1 back into Eq. (21) and solving it for h , we find the critical value of h_{AS} . Note again that, while the classical value of h_{AS} is constant at all scales, the strain

gradient theory predicts that the value of h_{AS} increases by scaling down the nano-structure, as shown in Fig. 5. This is also clear in Fig. 4a and 4b.

For finding the critical value of h which brings about the AR and AS points to the stable branches of the bifurcation diagram, thus making the sufficient condition for symmetry breaking, Eqs. (20) and (21) need to be satisfied simultaneously. Based on Fig. 4a, this happens at two points where the symmetric and asymmetric critical curves intersect. One of these points with positive q_1 represents the sufficient condition for asymmetric snap-through (TS), and the other point with negative q_1 stands for threshold asymmetric release (TR). Figure 4a shows that the normalized value of h corresponding to TS point is slightly smaller than that contributing to TR ($h_{TS} < h_{TR}$). Figure 5 displays the normalized values of h_{TS} versus various values of the d/Cl ratio. Corresponding constant classical values of h_S , h_{AS} and h_{TS} are shown as the inset in Fig. 5.

5 Analytical criteria

In this section, we aim to provide analytical expressions for prediction of the symmetric and asymmetric instabilities of the nano-arch. Referring to Fig. 4a, one can find that the critical value of q_1 associated with the minimum initial rise parameter needed for symmetric buckling, h_S , is close to zero. Medina et al. (2012) have shown that, for the case of an initially curved beam under deflection-independent loading provided by elastic foundation, such critical value of q_1 always equals to zero; but, for the case of deflection-dependent loading provided by the electrostatic actuation, this critical value of q_1 is not necessarily zero, while being small. Thus, we can make a good approximation for h_S by analytically solving Eq. (20) for h and evaluating it at $q_1 = 0$. Moreover, using Table 3 and the definition (4) with $G = \tilde{E}/2(1 + \nu)$, the size-dependent stretching parameter θ_1 is given by the following expression:

$$\theta_1 = \frac{6}{d^2 + 20n^2} \tag{22}$$

where d is the non-dimensional thickness given in Table 3, and $n = Cl/g$ which reflects size-dependency. However, using (22) and following the procedure described above, we obtain h_S by the following approximation:

$$h_S(d, n) = \kappa_1 (d^2 + 20n^2) \left(1 + \sqrt{1 + \frac{\chi_1}{d^2 + 20n^2}} \right), \tag{23}$$

$$\kappa_1 = \frac{I'_{10} b_{11}}{12s_{11}^2 I_{10}}, \quad \chi_1 = \frac{24s_{11}^2 I_{10}^2}{b_{11} I_{10}^2},$$

with I_{10} and I'_{10} representing the values of $I_1(q_1)$ and its derivative with respect to q_1 evaluated at $q_1 = 0$.

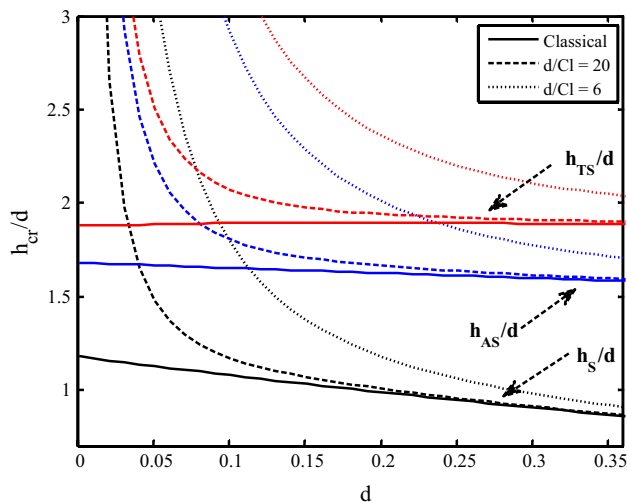


Fig. 6 Critical values of h/d ratio for symmetric snap-through (h_S/d in dark color), asymmetric snap-through (h_{AS}/d in blue), and threshold snap-through (h_{TS}/d in red). The results obtained by two values of d/Cl ratio are compared with the classical results at each case (color figure online)

Equation (23) yields size-dependent values of h_S , which are in good agreement with the numerically-obtained values given in Fig. 5. The ratio of h_S/d obtained from (23) for various values of d/Cl ratios is depicted in Fig. 6.

We can employ the same procedure for obtaining an expression for description of the necessary condition for possibility of symmetry breaking. Solving Eq. (21) for h and evaluating the result at $q_1 = 0$, replacing θ_1 from (22) and using Table 3, we are left with the following expression for h_{AS} :

$$h_{AS}(d, n) = \kappa_2(d^2 + 20n^2) \left(-1 + \sqrt{1 + \frac{\chi_2}{d^2 + n^2}} \right),$$

$$\kappa_2 = \frac{b_{11}I_{20}}{6s_{11}s_{22}I_{10}}, \chi_2 = \frac{6b_{22}s_{11}s_{22}I_{10}^2}{b_{11}^2I_{20}^2}, \quad (24)$$

where I_{20} is the value of $I_2(q_1)$ given by (18) and evaluated at $q_1 = 0$. Other parameters are as before. Values of h_{AS} given by (24) are in good agreement with the numerically-obtained values displayed in Fig. 5. Also, the size-dependent values of h_{AS}/d given by (24) are depicted in Fig. 6 for various values of the d/Cl ratio.

For the threshold value of parameter h , representing the sufficient condition for symmetry breaking, the analytical solution for the simultaneous Eqs. (20) and (21) is not available. Thus, for each scaled nano-arch, one can numerically solve these two concurrent equations for h , and select the smaller of the two obtained results as the threshold value for asymmetric snap-through h_{TS} . We have done this in Fig. 6 which illustrates the size-dependent values of h_{TS}/d for various values of the d/Cl ratio.

6 Conclusion

In this paper, we have investigated the size-dependent nature of symmetric and asymmetric nonlinear behaviors in an electrostatically actuated initially curved stress-free shallow nano-beam modeled by the strain gradient theory which is a continuum theory capable of incorporating with the size-effects. To this aim, we have derived a two-degree-of-freedom model by application of the Galerkin projection method to the partial differential equation given by the strain gradient theory. The obtained reduced-order model consists of the first symmetric and asymmetric mode shapes of the beam, and is capable to account for the beam instabilities as well as the size-dependencies.

Using the bifurcation diagrams of equilibrium points of the obtained reduced-order model, we have obtained the critical size-dependent snap-through, release and pull-in values of the DC voltage parameter. Moreover, we have obtained the minimum initial elevation parameter which is required for the possibility of symmetric or asymmetric buckling.

Our investigations show that, despite what is already proposed using the classical continuum models, the critical snap-through, release and pull-in points as well as the minimum initial elevation parameters required for the possibility of snap-through and symmetry breaking are all size-dependent. We have shown that as the nano-arch scales down, the critical values of the voltage parameter for the symmetric snap-through and pull-in decreases, while that of the symmetric release increases. Thus, the range of bistability shrinks as the nano-arch scales down, and the minimum initial elevation parameter required for the possibility of symmetric buckling increases at smaller sizes. Additionally, as the structure scales down, the possibility of symmetry breaking reduces, and the minimum initial elevation parameter required for the possibility of symmetry breaking increases. In the same way, the critical threshold value of the voltage and initial elevation parameters, which result in the initiation of asymmetric buckling prior to the symmetric snap-through, increase as the structure scales down. We have derived analytical expressions for the size-dependent critical values of initial elevation parameter required for symmetric and asymmetric buckling using the obtained reduced order model.

Results of this paper provide deep insight into the size-dependency of nonlinear dynamics in nano-scaled initially curved electrostatically actuated beams, and suggest that application of the conventional classical continuum models for the design of bistable nano-scaled NEMS can provide conservative or even inaccurate results. Further experimental investigations for validation of the obtained results are required and are left as future work.

Acknowledgements Funding was provided by Natural Sciences and Engineering Research Council of Canada (Grant No. 129619).

References

- Akgöz B, Civalek Ö (2013) Free vibration analysis of axially functionally graded tapered Bernoulli–Euler microbeams based on the modified couple stress theory. *Compos Struct* 98:314–322. doi:[10.1016/j.compstruct.2012.11.020](https://doi.org/10.1016/j.compstruct.2012.11.020)
- Alemansour H, Maani Miandoab E, Nejat Pishkenari H (2017) Effect of size on the chaotic behavior of nano resonators. *Commun Nonlinear Sci Numer Simul* 44:495–505. doi:[10.1016/j.cnsns.2016.09.010](https://doi.org/10.1016/j.cnsns.2016.09.010)
- Amini Khoiy K, Amini R (2016) On the biaxial mechanical response of porcine tricuspid valve leaflets. *J Biomech Eng* 138:104504. doi:[10.1115/1.4034426](https://doi.org/10.1115/1.4034426)
- Amini Khoiy K, Biswas D, Decker TN et al (2016) Surface strains of porcine tricuspid valve septal leaflets measured in ex vivo beating hearts. *J Biomech Eng* 138:111006. doi:[10.1115/1.4034621](https://doi.org/10.1115/1.4034621)
- Camescasse B, Fernandes A, Pouget J (2014) Bistable buckled beam and force actuation: experimental validations. *Int J Solids Struct* 51:1750–1757. doi:[10.1016/j.ijsolstr.2014.01.017](https://doi.org/10.1016/j.ijsolstr.2014.01.017)
- Charlot B, Sun W, Yamashita K et al (2008) Bistable nanowire for micromechanical memory. *J Micromech Microeng* 18:45005. doi:[10.1088/0960-1317/18/4/045005](https://doi.org/10.1088/0960-1317/18/4/045005)
- Chen J, Chang D (2007) Snapping of a shallow arch with harmonic excitation at one end. *J Vib Acoust* 129:514–519. doi:[10.1115/1.2748479](https://doi.org/10.1115/1.2748479)
- Das K, Batra RC (2009a) Pull-in and snap-through instabilities in transient deformations of microelectromechanical systems. *J Micro-mech Microeng* 19:35008. doi:[10.1088/0960-1317/19/3/035008](https://doi.org/10.1088/0960-1317/19/3/035008)
- Das K, Batra RC (2009b) Symmetry breaking, snap-through and pull-in instabilities under dynamic loading of microelectromechanical shallow arches. *Smart Mater Struct* 18:115008. doi:[10.1088/0964-1726/18/11/115008](https://doi.org/10.1088/0964-1726/18/11/115008)
- Farokhi H, Ghayesh MH, Amabili M (2013) Nonlinear dynamics of a geometrically imperfect microbeam based on the modified couple stress theory. *Int J Eng Sci* 68:11–23. doi:[10.1016/j.ijengsci.2013.03.001](https://doi.org/10.1016/j.ijengsci.2013.03.001)
- Fleck NA, Muller GM, Ashby MF, Hutchinson JW (1994) Strain gradient plasticity: theory and experiment. *Acta Metall Mater* 42:475–487
- Fu Y, Zhang J, Jiang Y (2010) Influences of the surface energies on the nonlinear static and dynamic behaviors of nanobeams. *Phys E Low Dimens Syst Nanostruct* 42:2268–2273. doi:[10.1016/j.physe.2010.05.001](https://doi.org/10.1016/j.physe.2010.05.001)
- Ghayesh MH, Farokhi H, Amabili M (2013) Nonlinear behaviour of electrically actuated MEMS resonators. *Int J Eng Sci* 71:137–155
- Intaraprasong V, Fan S (2011) Nonvolatile bistable all-optical switch from mechanical buckling. *Appl Phys Lett* 98:241104. doi:[10.1063/1.3600335](https://doi.org/10.1063/1.3600335)
- Kong S, Zhou S, Nie Z, Wang K (2009) Static and dynamic analysis of micro beams based on strain gradient elasticity theory. *Int J Eng Sci* 47:487–498. doi:[10.1016/j.ijengsci.2008.08.008](https://doi.org/10.1016/j.ijengsci.2008.08.008)
- Krylov S, Dick N (2010) Dynamic stability of electrostatically actuated initially curved shallow micro beams. *Contin Mech Thermodyn* 22:445–468. doi:[10.1007/s00161-010-0149-6](https://doi.org/10.1007/s00161-010-0149-6)
- Krylov S, Ilic BR, Schreiber D et al (2008) The pull-in behavior of electrostatically actuated bistable microstructures. *J Micromech Microeng* 18:55026. doi:[10.1088/0960-1317/18/5/055026](https://doi.org/10.1088/0960-1317/18/5/055026)
- Krylov S, Ilic B, Lulinsky S (2011) Bistability of curved microbeams actuated by fringing electrostatic fields. *Nonlinear Dyn* 66:403–426
- Lam DCC, Yang F, Chong ACM et al (2003) Experiments and theory in strain gradient elasticity. *J Mech Phys Solids* 51:1477–1508. doi:[10.1016/S0022-5096\(03\)00053-X](https://doi.org/10.1016/S0022-5096(03)00053-X)
- Maani Miandoab E, Yousefi-Koma A, Nejat Pishkenari H, Tajaddodianfar F (2014) Study of nonlinear dynamics and chaos in MEMS/NEMS resonators. *Commun Nonlinear Sci Numer Simul*. doi:[10.1016/j.cnsns.2014.07.007](https://doi.org/10.1016/j.cnsns.2014.07.007)
- Maani Miandoab E, Nejat Pishkenari H, Yousefi-Koma A (2015a) Dynamic analysis of electrostatically actuated nanobeam based on strain gradient theory. *Int J Struct Stab Dyn* 15:1450059. doi:[10.1142/S021945541450059X](https://doi.org/10.1142/S021945541450059X)
- Maani Miandoab E, Tajaddodianfar F, Nejat Pishkenari H, Ouakad HM (2015b) Analytical solution for the forced vibrations of a nano-resonator with cubic nonlinearities using homotopy analysis method. *Int J Nanosci Nanotechnol* 11:159–166
- Maani Miandoab E, Yousefi-Koma A, Nejat Pishkenari H, Tajaddodianfar F (2015c) Study of nonlinear dynamics and chaos in MEMS/NEMS resonators. *Commun Nonlinear Sci Numer Simul* 22:611–622. doi:[10.1016/j.cnsns.2014.07.007](https://doi.org/10.1016/j.cnsns.2014.07.007)
- Medina L, Gilat R, Krylov S (2012) Symmetry breaking in an initially curved micro beam loaded by a distributed electrostatic force. *Int J Solids Struct* 49:1864–1876. doi:[10.1016/j.ijsolstr.2012.03.040](https://doi.org/10.1016/j.ijsolstr.2012.03.040)
- Medina L, Gilat R, Ilic B, Krylov S (2014a) Experimental investigation of the snap-through buckling of electrostatically actuated initially curved pre-stressed micro beams. *Sens Actuators A Phys* 220:323–332. doi:[10.1016/j.sna.2014.10.016](https://doi.org/10.1016/j.sna.2014.10.016)
- Medina L, Gilat R, Krylov S (2014b) Symmetry breaking in an initially curved pre-stressed micro beam loaded by a distributed electrostatic force. *Int J Solids Struct* 51:2047–2061. doi:[10.1016/j.ijsolstr.2014.02.010](https://doi.org/10.1016/j.ijsolstr.2014.02.010)
- Mustapha KB, Ruan D (2015) Size-dependent axial dynamics of magnetically-sensitive strain gradient microbars with end attachments. *Int J Mech Sci* 94–95:96–110. doi:[10.1016/j.ijmecsci.2015.02.010](https://doi.org/10.1016/j.ijmecsci.2015.02.010)
- Namazu T, Isono Y, Tanaka T (2000) Evaluation of size effect on mechanical properties of single crystal silicon by nanoscale bending test using AFM. *J Microelectromech Syst* 9:450–459. doi:[10.1109/84.896765](https://doi.org/10.1109/84.896765)
- Nejat Pishkenari H, Afsharmanesh B, Tajaddodianfar F (2015) Continuum models calibrated with atomistic simulations for the transverse vibrations of silicon nanowires. *Int J Eng Sci* 100:8–24. doi:[10.1016/j.ijengsci.2015.11.005](https://doi.org/10.1016/j.ijengsci.2015.11.005)
- Plaut RH (2009) Snap-through of shallow elastic arches under end moments. *J Appl Mech* 76:14504. doi:[10.1115/1.3000020](https://doi.org/10.1115/1.3000020)
- Plaut RH (2015) Snap-through of arches and buckled beams under unilateral displacement control. *Int J Solids Struct*. doi:[10.1016/j.ijsolstr.2015.02.044](https://doi.org/10.1016/j.ijsolstr.2015.02.044)
- Reddy JN (2010) Nonlocal nonlinear formulations for bending of classical and shear deformation theories of beams and plates. *Int J Eng Sci* 48:1507–1518. doi:[10.1016/j.ijengsci.2010.09.020](https://doi.org/10.1016/j.ijengsci.2010.09.020)
- Seyranian AP, Elishakoff I (1989) *Modern problems of structural stability*. Springer, Vienna
- Simites GJ (1990) *Dynamic stability of suddenly loaded structures*. Springer, Berlin
- Southworth DR, Bellan LM, Linzon Y et al (2010) Stress-based vapor sensing using resonant microbridges. *Appl Phys Lett* 96:163503
- Tajaddodianfar F, Hairi Yazdi MR, Nejat Pishkenari H (2014a) Dynamics of bistable initially curved shallow microbeams: effects of the electrostatic fringing fields. In: 2014 IEEE/ASME international conference on advanced intelligent mechatronics. Besancon, France, pp 1279–1283
- Tajaddodianfar F, Hairi Yazdi MR, Nejat Pishkenari H, Maani Miandoab E (2014b) Nonlinear dynamics of electrostatically actuated micro-resonator: analytical solution by homotopy perturbation method. In: 2014 IEEE/ASME international conference

- on advanced intelligent mechatronics. Besancon, France, pp 1284–1289
- Tajaddodianfar F, Hairi Yazdi M, Nejat Pishkenari H (2015a) On the chaotic vibrations of electrostatically actuated arch micro/nano resonators: a parametric study. *Int J Bifurc Chaos* 25:1550106. doi:[10.1142/S0218127415501060](https://doi.org/10.1142/S0218127415501060)
- Tajaddodianfar F, Hairi Yazdi MR, Nejat Pishkenari H et al (2015b) Classification of the nonlinear dynamics in an initially curved bistable micro/nano-electro-mechanical system resonator. *Micro Nano Lett* 10:583–588. doi:[10.1049/mnl.2015.0087](https://doi.org/10.1049/mnl.2015.0087)
- Tajaddodianfar F, Nejat Pishkenari H, Hairi Yazdi M, Maani Mian-doab E (2015c) On the dynamics of bistable micro/nano resonators: analytical solution and nonlinear behavior. *Commun Nonlinear Sci Numer Simul* 20:1078–1089. doi:[10.1016/j.cnsns.2014.06.048](https://doi.org/10.1016/j.cnsns.2014.06.048)
- Tajaddodianfar F, Nejat Pishkenari H, Hairi Yazdi M, Maani Mian-doab E (2015d) Size-dependent bistability of an electrostatically actuated arch NEMS based on strain gradient theory. *J Phys D Appl Phys* 48:245503. doi:[10.1088/0022-3727/48/24/245503](https://doi.org/10.1088/0022-3727/48/24/245503)
- Tajaddodianfar F, Hairi Yazdi MR, Nejat Pishkenari H (2016a) Nonlinear dynamics of MEMS/NEMS resonators: analytical solution by the homotopy analysis method. *Microsyst Technol*. doi:[10.1007/s00542-016-2947-7](https://doi.org/10.1007/s00542-016-2947-7)
- Tajaddodianfar F, Nejat Pishkenari H, Hairi Yazdi MR (2016b) Prediction of chaos in electrostatically actuated arch micro-nano resonators: analytical approach. *Commun Nonlinear Sci Numer Simul* 30:182–195. doi:[10.1016/j.cnsns.2015.06.013](https://doi.org/10.1016/j.cnsns.2015.06.013)
- Wang J, Huang Q-A, Yu H (2008) Size and temperature dependence of Young's modulus of a silicon nano-plate. *J Phys D Appl Phys* 41:165406. doi:[10.1088/0022-3727/41/16/165406](https://doi.org/10.1088/0022-3727/41/16/165406)
- Wang B, Zhou S, Zhao J, Chen X (2011) Size-dependent pull-in instability of electrostatically actuated microbeam-based MEMS. *J Micro-mech Microeng* 21:27001. doi:[10.1088/0960-1317/21/2/027001](https://doi.org/10.1088/0960-1317/21/2/027001)
- Younis MI, Ouakad HM, Alsalem FM et al (2010) Nonlinear dynamics of MEMS arches under harmonic electrostatic actuation. *J Microelectromech Syst* 19:647–656
- Zhang Y, Wang Y, Li Z et al (2007) Snap-through and pull-in instabilities of an arch-shaped beam under an electrostatic loading. *J Microelectromech Syst* 16:684–693
- Zhang W-M, Yan H, Peng Z-K, Meng G (2014) Electrostatic pull-in instability in MEMS/NEMS: a review. *Sens Actuators A Phys* 214:187–218. doi:[10.1016/j.sna.2014.04.025](https://doi.org/10.1016/j.sna.2014.04.025)